

Fault-tolerant linear optics quantum computation by error-detecting quantum state transfer

Jaeyoon Cho

Leading-Edge Technology Group, Korea Research Institute of Standards and Science, Daejeon 305-340, Korea

(Dated: May 26, 2019)

A scheme for linear optical implementation of fault-tolerant quantum computation is proposed, which is based on an error-detecting code. Each computational step is mediated by transfer of quantum information into an ancilla system embedding error-detection capability. Photons are assumed to be subjected to both photon loss and depolarization, and the threshold region of their strengths for scalable quantum computation is obtained, together with the amount of physical resources consumed. Compared to currently known results, the present scheme reduces the resource requirement, while yielding a comparable threshold region.

One of the main obstacles to implementing a quantum computer using single-photon qubits is the lack of high nonlinearity between individual photons. Thanks to the development of the linear optics quantum computation (LOQC) scheme [1], we now believe that such a problem would be solved in terms of measurement-induced nonlinearity. Recently the demanding requirements of the original LOQC scheme have been significantly reduced by importing the idea of one-way quantum computation [2, 3, 4].

Although the LOQC approach seems to be quite promising, we are remained with another essential requirement for the practical realization: an ability to cope with inevitable physical noise originated from decoherence or imperfect operations. Fortunately, we are equipped with the ingenious theory of fault-tolerant quantum computation [5]. The main result of it is the threshold theorem which states that a scalable quantum computation can be performed with an arbitrary precision provided the noise strength is below a certain threshold [6, 7].

Applying the threshold theorem into the model of one-way quantum computation is not a trivial task. The main reason is that the threshold theorem is originally devised for the quantum circuit model. Recently, there have been reports on the existence of the fault-tolerant threshold for one-way quantum computation [8] and also on the estimation of its value [9, 10].

Concerning LOQC, however, it is more difficult to obtain the threshold result, since additional effects due both to the nondeterministic nature of optical two-qubit gates and to photon loss have to be taken into account. In Ref. [11], this issue was addressed and the fault-tolerant threshold was calculated by introducing an error-correction scheme tailored to LOQC. Although it is a remarkable result, the problem is that its resource requirement is extremely demanding. Therefore, there still remains much room for improvement in this regard.

In the present paper, a fault-tolerant LOQC scheme using an error-detecting code is proposed. In the quantum circuit model, a fault-tolerant quantum computation using an error-detecting code generally tends to consume

more resources than that using an error-correcting code [7]. In the present scheme, however, the resource consumption is decreased in many orders of magnitude compared to the known results using error-correcting codes, without the expense of decreasing the tolerable noise level.

Physical model and noise.—The present scheme is on the same footing as recent investigations of LOQC based on one-way quantum computation. The details concerning the physical model and noise are omitted here. In short summary, we make use of a sufficient amount of two-photon polarization-entangled Bell states, linear optical elements, and number-resolving photodetectors. An elementary gate extensively used is the (type-I) fusion gate [4]. The noise model is employed from Ref. [11] for direct comparison of results: each operation takes one unit time step, and is modeled as a noiseless one accompanied with noise acting appropriately before or after it. Two types of noise are taken into account. At each noise location, each photon is lost independently with probability γ and depolarization occurs as follows: for one-qubit operations, one of 3 Pauli errors is applied each with probability $\epsilon/3$, and for two-qubit operations, one of 15 non-identity Pauli products is applied each with probability $\epsilon/15$. Conventional assumptions of independent noise, nonlocal gates, maximum parallelism, and fast error-free classical processing are also made.

Pauli frame.—Instead of implementing Pauli operators X , Z , and $Y = iZX$ physically, we just keep track of the product of Pauli operators which should have been applied to the state. This Pauli product is called the Pauli frame [7, 11]. The Pauli frame is updated after each operation according to the quantum circuit identities. This is possible since we use the Clifford gates that transform Pauli operators into Pauli operators under conjugation.

Error-detecting code and encoded operations.—We use a 4-qubit stabilizer code, which is stabilized by three operators: $\bar{S}_1 = X_1X_2X_3X_4$, $\bar{S}_2 = Z_1Z_2I_3I_4$, and $\bar{S}_3 = I_1I_2Z_3Z_4$, where X_i and Z_i are the Pauli operators and I_i is the identity operator acting on the i th qubit. Since the distance of this code is two, it detects one error. The encoded Pauli operators are cho-

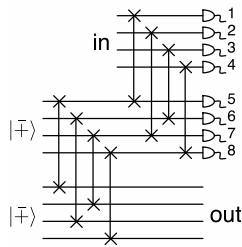


FIG. 1: Quantum circuit for error-detecting quantum state transfer.

sen to be $\bar{X} = X_1X_2I_3I_4$ and $\bar{Z} = Z_1I_2Z_3I_4$. This choice makes it simple to generate an encoded state $|\bar{\pm}\rangle$ ($+1$ eigenstate of \bar{X}), since it decomposes into two Bell states. Each Bell state is generated by measuring the middle qubit of a linear three-qubit cluster state in the X basis, which is a fault-tolerant process thanks to the symmetry of Bell states. The encoded CPHASE operation is performed by four disjoint CPHASE operations as $U(1,5)U(2,7)U(3,6)U(4,8)$, where $U(i,j)$ denotes CPHASE between qubits i and j , and two encoded qubits are represented, respectively, by qubits 1 to 4 and 5 to 8. The measurement of the encoded operator \bar{X} or \bar{Z} is performed by measuring each of the four qubits in the same basis of X or Z . Note that these measurements give redundant information. For example, the value of the \bar{X} -basis measurement is given either by the measurement of X_1X_2 or X_3X_4 . This redundancy plays an important role in the code concatenation described later.

Error-detecting quantum state transfer.—Fig. 1 depicts a quantum circuit for an encoded memory gate. Two encoded ancilla qubits are first prepared in a cluster state and then connected to an encoded input qubit through an encoded CPHASE gate. We then measure both the input qubit and the next ancilla qubit in the \bar{X} basis. It is easily seen that this process simply transfers the encoded input state to the last encoded ancilla qubit up to the Pauli frame correction [2]. An important insight into this process, which we will call the error-detecting quantum state transfer, is that it also embeds the syndrome information into the measurement results. Suppose first that the quantum circuit of Fig. 1 is error-free. If one of the input qubits has an X error, the corresponding value among those of measurements 5 to 8 is flipped, which leads to the parity of the four measurement values being odd. In the same way, one Z error in the input leads to the parity for the measurement of $X_1X_2X_3X_4$ being odd. One can easily check that an error at any one location of the whole circuit is also indicated by the parity checks, or possibly by the next round of error-detecting quantum state transfer. The idea outlined here can be expanded so that an encoded operation is embedded into the ancilla preparation, as will be described later.

Code concatenation.—We make use of the standard technique of code concatenation, whose hierarchy ranges

from level 0 (where a qubit is encoded in one photon) to level l_d (where a qubit is encoded in 4^{l_d} photons). Individual operations in each level are characterized with two statistical quantities: the located and the unlocated error rates. The located error rate is defined as the probability that for a particular input state the embedded error-detecting process detects an error, and the unlocated error rate is defined as the probability that, while the error-detecting process fails to detect an error, the final state still has an error which can not be detected even with perfect error-detecting quantum state transfer (an analogous definition is used for the measurement). The aim of code concatenation is to obtain sufficiently low error rates in the topmost level. Unfortunately, applying conventional concatenation methods directly to our scheme is not impractical. We thus define two modes of error-detecting quantum state transfer, namely, the strong- and the weak-detection modes. In the strong-detection mode, any event of detecting an error during the whole process is interpreted as an occurrence of a located error, while in the weak-detection mode, one located error during the final time step is allowed by actively exploiting the redundancy of the \bar{X} -basis measurement. For example, if a located error occurs during the CPHASE operation corresponding to measurements 2 and 7 in Fig. 1, instead of discarding the operation, we use the results of measurements 3, 4 and 5, 6 to obtain the values of the \bar{X} -basis measurements. In this way, we get a lower located error rate at the expense of a higher unlocated error rate. The underlying idea behind these two modes is that we take advantage of the low unlocated error rate of the strong-detection mode for the ancilla preparation, while we use the weak-detection mode for the operations between ancilla and input states in order to reduce the chance of discarding the computation.

Universal set of quantum gates.—The universal quantum computation is guaranteed by bringing in the preparation of state $|\pi/8\rangle = \cos(\pi/8)|0\rangle + \sin(\pi/8)|1\rangle$ which allows the implementation of the $\pi/8$ gate $T = \exp(-i\frac{\pi}{8}Z)$, where $|0\rangle$ and $|1\rangle$ are the eigenstates of Z . In order to prepare the $|\pi/8\rangle$ state, we first prepare a Bell state in the topmost level. We then measure one of the two qubits in the basis of $\{|\pi/8\rangle, |5\pi/8\rangle\}$, where $|5\pi/8\rangle = ZX|\pi/8\rangle$ is the state orthogonal to the $|\pi/8\rangle$ state. This measurement is done by measuring the corresponding lower-level qubits, respectively, in the bases of Z , Z , X , and $\{|\pi/8\rangle, |5\pi/8\rangle\}$, the last of which is, in turn, done by measuring the lower-level qubits in the same way. As a result, the other qubit in the topmost level is remained in the $|\pi/8\rangle$ state up to the Pauli frame correction. Note that errors occurring during the measurement could introduce an error in the topmost level, but they do not destroy the encoding structure. We can thus purify multiple copies of noisy $|\pi/8\rangle$ states in the topmost level [7, 12].

Level-0 encoding.—Quantum state transfer in the bot-

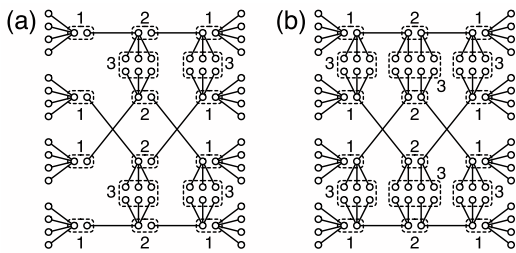


FIG. 2: Cluster states for the level-1 memory (a) and Bell-state preparation (b). Fusion gates are applied in the order indicated by the numbers.

tom level relies on microclusters and parallel fusion as outlined in Ref. [11]. Quantum information is stored in the center node of a star-shaped cluster state, called a microcluster. In order to transfer the state of one center node, say qubit 1, to another center node, say qubit 2, we apply fusion gates pairwise between the dangling nodes in parallel, and measure qubit 1 and all successfully fused nodes in the X basis. If two or more fusion operations were successful, all of the following measurements should have the same value. If it is not the case, we conclude that qubit 2 has an error. We also come to the same conclusion if any of the involved operations indicates a photon loss. If we ignore noise, the success probability of the parallel fusion increases exponentially as the number of dangling nodes increases. More dangling nodes, however, introduce more noise and thus decrease the success probability asymptotically. In the present paper, the number of dangling nodes of each microcluster is fixed as 4. We always regard a fusion gate and the following X -basis measurement as being performed in one time step, since it can be done by measuring both the output photons of the polarizing beam splitter in the X basis.

Level-1 encoding.—Fig. 2(a) depicts the cluster state to simulate a level-1 memory gate. Each circle represents a single-photon qubit. Fusion gates are applied in the order indicated by the numbers. The resulting cluster state is then composed of three columns, each representing a level-1 qubit, and the dangling nodes at both sides (leftmost nodes for input and rightmost nodes for output). It is easily seen that the quantum circuit simulated by this cluster state is equivalent to that of error-detecting quantum state transfer shown in Fig. 1. All qubits in the three columns are measured in the X basis. Note that these measurements can be done even before an input state is fused (an analogous idea is used for the telecorrector introduced in Ref. [11]). Actually, each measurement is performed together with a preceding fusion gate in one time step as explained earlier. If any of the fusion gates or the measurements indicates a photon loss, this preparation stage is restarted. Otherwise, the resulting state is accepted and finally fused with a level-1 input qubit on the left side. Note that the measurements in the right-

most column do not give information about the encoded state, since it is transferred to the rightmost dangling nodes. For an X -basis measurement, we construct the same cluster state without the rightmost dangling nodes. In this case, the measurement parity of the rightmost column is not altered by the Pauli frame correction after an input qubit is fused. We thus restart the preparation stage if the parity is found to be odd. A CPHASE operation is performed in a similar way by constructing a cluster state composed of six columns of qubits, say columns 1 to 6. In this case, columns 1 and 6 have dangling nodes for the input, while columns 3 and 4 have dangling nodes for the output. If measurements follow a CPHASE gate, they are also embedded into the preparation stage. For example, if the first output qubit of a CPHASE gate is measured, we construct a cluster state composed of six columns with dangling nodes attached to columns 1, 4, and 6, and the measurement parity of column 3 is used to filter out noisy ancilla states. Another useful operation is the Bell-state preparation shown in Fig. 2(b), which will be used for the preparation of a level-2 $|+\rangle$ state ($+1$ eigenstate of X). The resulting state is accepted unless any photon loss is detected or the measurement parity of the middle column is found to be odd.

Second and higher levels of encoding.—Our CHPASE gate has a useful property that two qubits can be input at different time steps. We take advantage of this property in the level- l ($l \geq 2$) encoding as follows. In order to implement error-detecting quantum state transfer in Fig. 1, we first implement the ancilla part up to a half of the final gates (CPHASE plus measurement) corresponding to measurements 5 to 8, while the input dangling nodes at the other half are left untouched. Only when this preparation stage is successful, an input qubit is finally fused. During this time step, the output dangling nodes are left untouched. This method greatly reduces the located error rates of level- l gates, but introduces idle time steps of dangling nodes causing additional level-0 memory noises. Note that these noises accumulate as the level of encoding gets higher. After the accumulated noise exceeds a certain bound, additional levels of concatenation will make things worse rather than better. Therefore, this method is used only until we get sufficiently low error rates, and in the higher levels of encoding, we proceed with the implementation normally without the delayed fusion.

Fault-tolerant threshold and resource consumption.—The located and unlocated error rates of individual operations are calculated starting from a given set of parameters $\{\gamma, \epsilon\}$ with the help of numerical methods outlined in Ref. [11], together with analytical calculations for high levels of encoding. When the error rates asymptotically go to zero as the level of encoding gets higher, the given set is said to be within the threshold region. In our case, to find out such an asymptotic behavior involves exhaustive calculations due to the accumulated noises. For simplicity, we define one particular suffi-

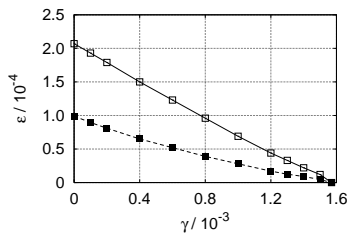


FIG. 3: Threshold region for scalable quantum computation using method 1 (solid curve) and method 2 (dotted curve), where γ and ϵ denote, respectively, the probabilities of photon loss and depolarization per operation.

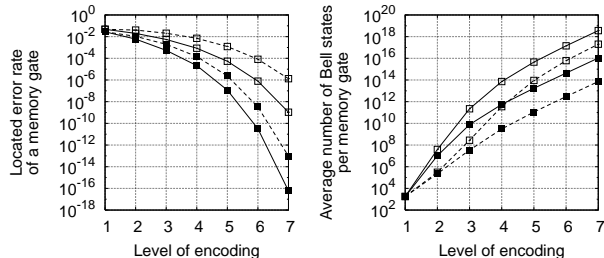


FIG. 4: Located error rate of a memory gate (left) and average number of two-photon Bell states consumed for it (right) with respect to the level of encoding.

cient condition (which will obviously lead to an excessively pessimistic estimation) as our fault-tolerance criterion: we say the set $\{\gamma, \epsilon\}$ is within the threshold region if the error rates of the level-5 operations satisfy all of the following conditions: $\max\{Q^M, Q^S\} \leq 10^{-2}$, $\max\{P_X^B, P_Z^B, 100P_Y^B\} \leq 10^{-6}$, $\max\{P_X^M, P_Z^M, 100P_Y^M\} \leq 10^{-4}$, and $\max\{P_X^S, P_Z^S, 100P_Y^S\} \leq 10^{-4}$, where Q and P denote, respectively, located and unlocated error rates, subscripts X , Y , and Z denote which Pauli error the unlocated error results in, and superscripts B , M , and S denote, respectively, Bell-state preparation, memory, and measurement. Every operations including a CPHASE gate can be modeled, with a good approximation, as noiseless ones preceded by relevant memory or measurement noises applied independently to each qubit. Provided these conditions are met, the error rates in the higher levels can be reduced asymptotically to zero without the need of delayed fusion. The error rates and the resource consumption vary according to how the strong- and the weak-detection modes are combined into code concatenation. Here, we consider two methods. In the first method, the ancilla part of a level- l operation is constructed with strongly-detected level- $(l-1)$ operations, while the remaining part is implemented with weak-detected level- $(l-1)$ operations. This strategy is iterated up to the topmost level, in which weakly-detected operations are used for real computation. The second method is the same as the first method except the ancilla part of a level-2 operation is constructed with weakly-detected level-1 operations. Compared to the first method, the

second method needs less resources for the same level of concatenation, but leads to higher error rates. The threshold regions for the first method (solid curve) and the second method (dotted curve) are shown in Fig. 3. We also plot in Fig. 4 the located error rate of a memory gate (left) and the resource consumption for it in terms of the average number of two-photon Bell states used (right) with respect to the level of encoding for the first method (solid curve) and the second method (dotted curve) with two sets of parameters: $\gamma = 10\epsilon = 4 \times 10^{-4}$ (unfilled squares) and $\gamma = 10\epsilon = 10^{-4}$ (filled squares). Located error rates always dominate unlocated error rates, thus indicate how many operations can be performed reliably. Compared to the results of Ref. [11] using error-correcting codes, our scheme requires in general less resources, while yielding comparable threshold regions. In case of $\gamma = 10\epsilon = 4 \times 10^{-4}$, we obtain the error rate of 10^{-9} using about 4×10^{18} Bell pairs (the first method), while the scheme in Ref. [11] requires about 10^{23} Bell pairs. The required resources are drastically reduced as the noise strength decreases. For example, in case of $\gamma = 10\epsilon = 10^{-4}$, the same error rate is attained using about 10^{13} Bell pairs (the second method). Although these results show great improvements, the resource requirement is still very large. It could be further reduced by simply changing the number of dangling nodes or by importing other techniques such as purification or error correction.

This research was supported by the "Single Quantum-Based Metrology in Nanoscale" project of the Korea Research Institute of Standards and Science.

-
- [1] E. Knill, R. Laflamme and G. J. Milburn, *Nature* **409**, 46 (2001).
 - [2] R. Raussendorf and H. J. Briegel, *Phys. Rev. Lett.* **86**, 5188 (2001).
 - [3] M. A. Nielsen, *Phys. Rev. Lett.* **93**, 040503 (2004).
 - [4] D. E. Browne and T. Rudolph, *Phys. Rev. Lett.* **95**, 010501 (2005).
 - [5] P. W. Shor, in *Proceedings of the 37th Annual Symposium on Foundations of Computer Science* (IEEE Press, Los Alamitos, CA, 1996), pp. 56-65; D. Aharonov and M. Ben-Or, in *Proceedings of the 29th Annual ACM Symposium on Theory of Computing (STOC)* (ACM, New York, 1997).
 - [6] A. M. Steane, *Phys. Rev. A* **68**, 042322 (2003).
 - [7] E. Knill, *Nature* **434**, 39 (2005).
 - [8] M. A. Nielsen and C. M. Dawson, *Phys. Rev. A* **71**, 042323 (2005).
 - [9] P. Aliferis and D. W. Leung, *Phys. Rev. A* **73**, 032308 (2006).
 - [10] R. Raussendorf and J. Harrington, *quant-ph/0610082*.
 - [11] C. M. Dawson, H. L. Haselgrove and M. A. Nielsen, *Phys. Rev. Lett.* **96**, 020501 (2006); C. M. Dawson, H. L. Haselgrove and M. A. Nielsen, *Phys. Rev. A* **73**, 052306 (2006).
 - [12] S. Bravyi and A. Kitaev, *Phys. Rev. A* **71**, 022316 (2005).